The insights from theoretical calculation on the photophysical properties of a series of phosphorescent iridium(III) complexes

Deming Han[a,b] & Jingmei Li[a]*

[a]School of Life Science and Technology, Changchun University of Science and Technology, Changchun 130022, P. R. China
[b]Jilin Provincial Science and Technology Innovation Center of Optical Materials and Chemistry, Changchun, 130022, P. R. China

Email: ljmljmcust@163.com

The electronic structure and photophysical properties of three Ir(III) complexes with the substituted 5,5′-di(trifluoromethyl)-3,3′-bipyrazole(bipz) ligand have been theoretically investigated by using density functional theory and time-dependent density functional theory method. The calculated results show that the energy gaps between of LUMO and HOMO ($\Delta E_{L \rightarrow H}$) of complexes **1**, **2** and **3** are gradually decreased, that is, 3.54 eV, 3.07 eV and 2.95 eV for **1**, **2** and **3**, respectively. The lowest energy absorption wavelength of **1**, **2** and **3** are located at 443 nm, 532 nm and 564 nm, respectively. The calculated 443 nm absorption for **1** is in good agreement with the experimental value. The lowest energy emissions of complexes **1, 2** and **3** are localized at 545 nm, 679 nm and 731 nm, respectively, simulated in CH_2Cl_2 medium at TPSSH level. The conclusion can be drawn that the different substituent groups in the bipz ligand results in the important effect on the electronic structure and photophysical properties. The research work can provide valuable information for the design of new organic light-emitting diodes materials.

Keywords: Photophysical property, DFT and TDDFT method, Iridium complex, Phosphorescence

As a new flat panel display technology, organic light-emitting diodes (OLEDs) has attracted great attention due to its advantages of all solid state, self-luminous, high brightness, wide viewing angle and fast response[1–6]. Recent years, the phosphorescent transition metal complexes such as Ru(II), Rh(III), Os(II), Ir(III) and Pt(II) complexes have received great interest due to their potential applications in the fabrication of OLEDs[7–11]. Especially, Ir(III) complexes are the most promising phosphorescent materials mainly owing to the excellent thermal stability, high photoluminescence quantum efficiency, short lifetime and flexible color adjustment[12–17]. The phosphorescence Ir(III) complexes can harvest both singlet and triplet excitons as light, leading to obtain an efficiency four times higher than fluorescent materials[18,19]. By changing the substituents on the main ligand or auxiliary ligand, the electronic structure and photophysical properties can be effectively adjusted[20–23]. For example, a series of bis(2′,6′-difluoro-2,3′-bipyridinato-N,C4′)iridium (picolinate) complexes [(dfpypy)₂Ir(pic): Ir1–Ir5] with different electron-withdrawing (–CHO, –CF₃ and –CN) and electron-donating substituents (–OMe and –NMe₂) on the 4′ position at the pyridyl moiety of the 2′,6′-difluoro-2,3′-bipyridine ligands has been synthesized, well characterized and investigated their photophysical properties by Bejoymohandas and co-workers[24].

Liao *et al.* have synthesized and characterized a series of Ir(III) metal-based phosphors with three bidentate chelates that consist of diimine, cyclometalate, and bis-pyrazolate[25]. On the basis of complex [Ir(dtbbpy)(ppy)][25], we have designed two new Ir(III) complexes by changing the substituents on the bipz ligand. To investigate the effect of substituent groups on photophysical properties, these iridium(III) complexes have been theoretically studied by using the density functional theory (DFT) and time-dependent density functional theory (TDDFT) method. The theoretical results will be useful for obtaining the good phosphorescent materials in OLEDs.

Materials and Methods

Computational method

The ground state geometry for each molecule was optimized by DFT[26] method with hybrid Hartree-Fock/density functional model (PBE0) based on the Perdew-Burke-Erzenrhof (PBE)[27]. On the basis

of the ground- and excited-state equilibrium geometries, the TDDFT approach was applied to investigate the absorption and emission spectral properties. The "double-ξ" quality basis set LANL2DZ[28,29] associated with the pseudopotential was employed on atom Ir. The 6–31G(d,p) basis set was used for nonmetal atoms in the gradient optimizations. Furthermore, the stable configurations of these complexes can be confirmed by frequency analysis, in which no imaginary frequency was found for all configurations at the energy minima. All calculations were performed with the polarized continuum model (PCM) in CH_2Cl_2 medium, which is adopted by Liao et al.[25]. The calculated electronic density plots for frontier molecular orbitals were prepared by using the GaussView 5.0.8 software. All calculations were performed with the Gaussian 09 software package[30]. The GaussSum2.5 was used to analyze the UV-visible absorption spectral properties[31].

Results and Discussion

Geometries in the ground state S_0 and triplet excited state T_1

The sketch map of complexes **1**, **2** and **3** are presented in Fig. 1(a), and the optimized ground state geometric structure for 1 is shown in Fig. 1(b) along
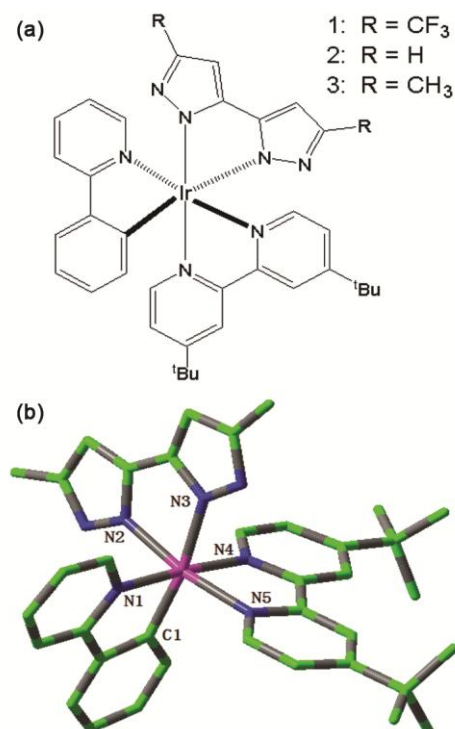

Fig. 1 — (a) Sketch map of the structures of complexes **1**, **2** and **3** and (b) Partial atomic number of complex **1** (H atoms omitted).

with the numbering of some key atoms. Complexes **1**, **2** and **3** show a distorted octahedral configuration because of the d^6 electronic configuration of Ir(II) atom. Table 1 listed the main optimized geometric parameters of S_0 and T_1 in order to better understand the structural change.

The bond lengths of Ir–N2 and Ir–N3 for all studied complexes are 2.03 Å and 2.13 Å, respectively. The bond lengths of Ir–N5 for all studied complexes are 2.05 Å. The bond angles C1–Ir–N3, N1–Ir–N4 and N2–Ir–N5 are larger than 170°, which is close to the straight angle 180°. In addition, the bond angle N1–Ir–N4 is larger than those of C1–Ir–N3 and N2–Ir–N5. For example, the C1–Ir–N3, N1–Ir–N4 and N2–Ir–N5 of complex **1** are 171.54°, 175.82° and 171.44°. The dihedral angles C1–N2–N3–N5, N1–N2–N4–N5 and C1–N4–N3–N1 are smaller than 9°. The above-mentioned results show that these complexes have the distorted octahedral configuration. On the whole, for the triplet excited state T_1, the bond distances are slightly changed in contrast to those in the ground state S_0. The bond angles C1–Ir–N3 and N2–Ir–N5 are slightly larger compared with those in S_0. The dihedral angle C1–N2–N3–N5 in T_1 state is obviously smaller than that in S_0.

Molecular orbital properties

The frontier molecular orbital (FMO) properties in the S_0 are closely related to the photophysical properties of these complexes. The HOMO (highest occupied molecular orbital) and LUMO (lowest unoccupied molecular orbital) distribution, energy levels, and energy gaps between of LUMO and HOMO ($\Delta E_{L\rightarrow H}$) of the complexes **1**, **2** and **3** are plotted in Fig. 2. The detailed information of FMO compositions for **1**, **2** and **3** have been presented in Tables S1–S3 (Supplementary Data).

The HOMO and LUMO distributions for complexes **1**, **2** and **3** are mainly located at the bipz and dtbbpy ligands, respectively. For example, the HOMO and LUMO of complex **1** distributes over the π-orbital of bipz (93%) and the π-orbital of dtbbpy (95%). From **1** to **3**, the HOMO and LUMO energy levels are gradually increased with the increasing electron-donating ability of substituent group in the bipz ligand. Especially, the HOMO energy levels have the more obvious change than those of LUMO, which causes the gradually reduced $\Delta E_{L\rightarrow H}$ values, that is, 3.54, 3.07, 2.95 eV for complexes **1**, **2**, and **3**, respectively. The investigation

Table 1 — Main optimized geometry parameters for complexes 1, 2 and 3

	1		2		3	
	S_0	T_1	S_0	T_1	S_0	T_1
bond length (Å)						
Ir–C1	2.01	2.00	2.02	2.00	2.02	2.00
Ir–N1	2.05	2.07	2.05	2.06	2.05	2.06
Ir–N2	2.03	2.03	2.03	2.04	2.03	2.04
Ir–N3	2.13	2.15	2.13	2.15	2.13	2.15
Ir–N4	2.03	2.03	2.02	2.03	2.03	2.03
Ir–N5	2.05	2.03	2.05	2.03	2.05	2.04
bond angle (°)						
C1–Ir–N3	171.54	172.84	170.87	172.71	171.22	172.82
N1–Ir–N4	175.82	174.59	175.78	174.63	175.77	174.64
N2–Ir–N5	171.44	172.52	170.24	171.98	170.22	171.99
dihedral angle (°)						
C1–N2–N3–N5	6.96	4.58	8.54	5.14	8.22	5.32
N1–N2–N4–N5	7.12	7.55	7.62	7.88	7.87	7.81
C1–N4–N3–N1	5.69	5.96	5.75	5.81	5.50	5.66
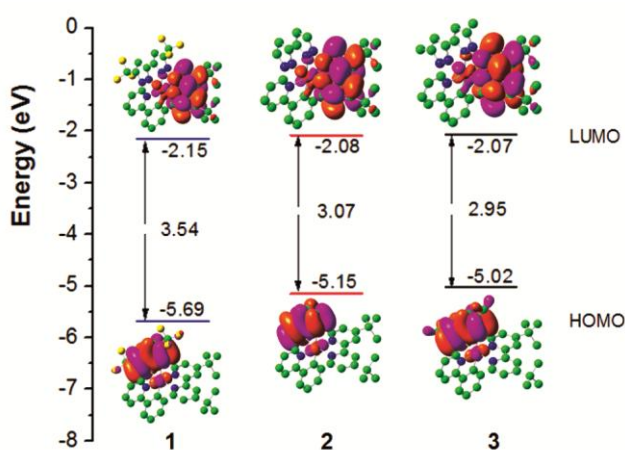
Fig. 2 — Molecular orbital diagrams and HOMO and LUMO energies for complexes 1, 2 and 3.

Fig. 3 — Simulated absorption spectra in CH_2Cl_2 medium for complexes 1, 2 and 3.

on the $\Delta E_{L\rightarrow H}$ values will be useful for studying the variation trend of the absorption.

Absorption spectra

The absorption properties of complexes 1, 2 and 3 have been calculated by using the PCM–TD–PBE0 method on the basis of the S_0 state geometries. The vertical electronic excitation energies, oscillator strengths (*f*), dominant orbital excitations and their assignments of singlet excited states have been listed in Table S4 (Supplementary Data). The stimulated absorption spectra of complexes 1, 2 and 3 in CH_2Cl_2 medium has been presented in Fig. 3.

As shown in Table S4, the lowest energy absorption wavelengths of 1, 2 and 3 are located at 443 nm (*f* = 0.0135), 532 nm (*f* = 0.0023) and 564 nm (*f* = 0.0022), respectively. The absorption

wavelength of 1 is comparable to the experimental observation[25]. It can be seen that the lowest energy absorption wavelengths are obviously redshifted in the order of 1→2→3, which is consistent with the variation of the ΔE_{L-H} values. This indicates that the electron-donating substituent group in the bipz ligand has the important effect on the absorption properties. Complex 1 has the strongest absorption peaks at ca. 228 and 268 nm. The absorption curve shapes of 2 and 3 are very similar. The lowest lying absorptions for complexes 1, 2 and 3 mainly have the HOMO→LUMO transition configuration contributing to the S_0→S_1 state. The lowest energy absorptions of complexes 1, 2 and 3 are characterized as ligand-to-ligand charge transfer (LLCT) [π (bipz)→ π *(dtbbpy)] character.

Phosphorescence in CH$_2$Cl$_2$ medium

To check the computational method, seven different density functionals (B3LYP, CAM-B3LYP, BP86, PBE1PBE, M052X, M062X and TPSSH) were used to calculate the emission of complex **1**. A better agreement with experimental data was obtained for TPSSH relative to other six functionals. The calculated emission energies for **1** at B3LYP, CAM-B3LYP, BP86, PBE1PBE, M052X, M062X and TPSSH levels are 489, 427, 683, 459, 394, 368 and 545 nm, respectively, with the deviations of 57, 119, 137, 87, 152, 178 and 1 nm deviating from measured value 546 nm[25]. Apparently, the TPSSH functional yields more satisfactory result. Hence, we have adopted the TPSSH functional for further emission spectra calculations. On the basis of the optimized triplet excited-state geometries, the emission properties of complexes **1**, **2** and **3** in CH$_2$Cl$_2$ solution obtained using the TDDFT method are shown in Table 2. The plots of the molecular orbitals related to emissions of complexes **1**, **2** and **3** are presented in Table 3. Besides, partial frontier molecular orbital compositions (%) of complexes

**1**, **2** and **3** in the triplet excited states have also been presented in Table S5.

Table 3 shows that the calculated lowest energy emissions of complexes **1**, **2** and **3** are located at 545, 679 and 731 nm, respectively. So, the lowest energy emissions of complexes **2** and **3** are obviously redshifted in contrast to that of **1**, which indicates the electron-donating substituent group in the bipz ligand can possess an important role. The reason for the large red shift of emission may be attributed to the limitation of the TDDFT method as shown by Świderek et al.[32], that is, high-energy excitations are not described by the TDDFT method. The lowest emissions for the three complexes are described as triplet ligand-to-ligand charge transfer (^{3}LLCT) [π*(dtbbpy)→π(bipz)]. The phosphorescence is mainly from the transitions of LUMO→HOMO configuration, which shows the different substitutents do not change the order between the frontier orbitals in emissions. As shown in Table 3 and Table S5, the HOMO and LUMO of the three complexes are mainly localized on the bipz and dtbbpy ligands, respectively. For example, the HOMO and LUMO distribution of complex **1** is on the bipz ligand (93%) and dtbbpy ligand (94%).

Table 2 — Phosphorescent emissions of complexes **1**, **2** and **3** in tetrahydrofuran at the TDDFT calculations, together with the experimental wavelength (nm) available

	λ(nm)/E(eV)	Configuration	Assignment	Nature	Expt.[a]
1	545/2.27	L→H (95%)	π*(dtbbpy)→π(bipz)	^{3}LLCT	546[a]
2	679/1.83	L→H (99%)	π*(dtbbpy)→π(bipz)	^{3}LLCT	
3	731/1.70	L→H (99%)	π*(dtbbpy)→π(bipz)	^{3}LLCT	

[a] Ref. 25

Table 3 — Transitions responsible for the emissions at 545, 679 and 731 nm for complexes **1**, **2** and **3**, respectively, simulated in CH$_2$Cl$_2$ medium
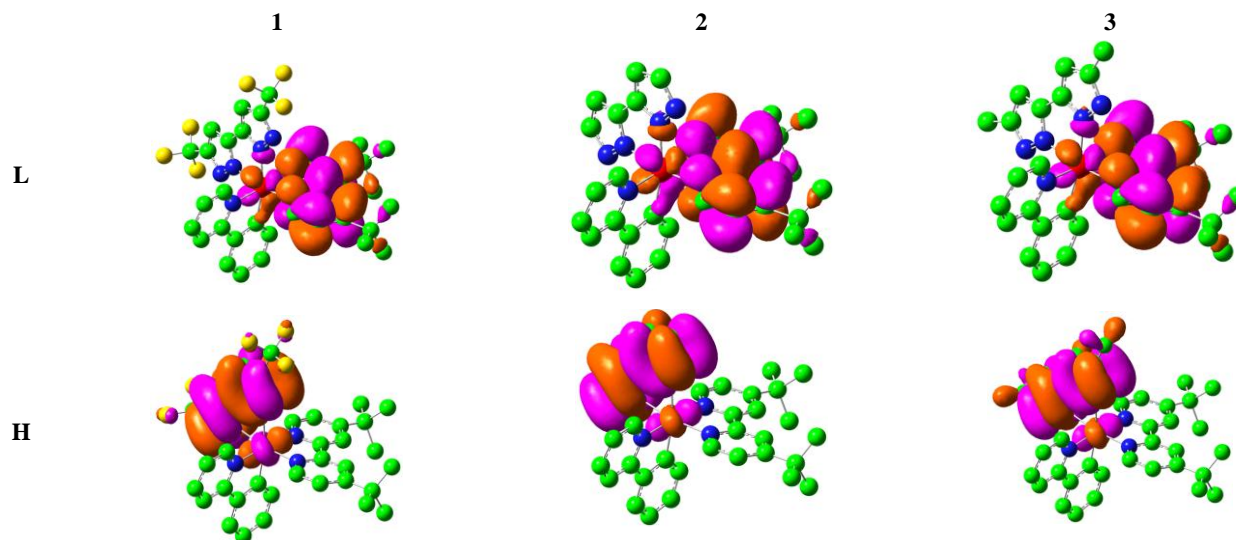
Conclusions

By using DFT/TDDFT method, the electronic structure and photophysical properties of three Ir(III) complexes have been explored in order to study the effect of the different substituent groups in the bipz ligand. The three complexes show a distorted octahedral configuration and similar ligands. The HOMO and LUMO for these complexes mainly distribute at the bipz and dtbbpy ligands, respectively. The lowest energy absorption wavelengths are in the order of **1** < **2** < **3**. The calculated lowest energy emission of **1** at TDDFT/TPSSH level is in agreement with the experimental value. The phosphorescence emission is mainly from the transitions of LUMO→HOMO configuration, which the HOMO and LUMO are most localized on the bipz and dtbbpy ligands, respectively. We hope that the study can provide a new perspective toward designing phosphorescent Ir(III) complexes for OLEDs materials.

Acknowledgments

References

1 Nasiri S, Cekaviciute M, Simokaitiene J, Petrauskaite A, Volyniuk D, Andruleviciene V, Bezvikonnyi O & Grazulevicius J V, *Dyes Pigments*, 168 (2019) 93.
2 Abdurahman A, Chen Y X, Ai X, Ablikim O, Gao Y, Dong S Z, Li B, Yang B, Zhang M & Li F, *J Mater Chem C*, 6 (2018) 11248.
3 Benjamin H, Fox M A, Batsanov A S, Al-Attar H A, Li C S, Ren Z J, Monkman A P & Bryce M R, *Dalton Trans*, 46 (2017) 10996.
4 Taydakov I V, Akkuzina A A, Avetisov R I, Khomyakov A V, Saifutyarov R R & Avetissov I C, *J Lumin*, 177 (2016) 31.
5 Kaji H, Suzuki H, Fukushima T, Shizu K, Suzuki K, Kubo S, Komino T, Oiwa H, Suzuki F, Wakamiya A, Murata Y & Adachi C, *Nat Commun*, 6 (2015) 8476.
6 Malissa H, Kavand M, Waters D P, van Schooten K J, Burn P L, Vardeny Z V, Saam B, Lupton J M & Boehme C, *Science*, 345 (2014) 1487.
7 Hu Y F, Maclennan A & Sham T K, *J Lumin*, 166 (2015) 143.
8 Wei F F, Lai S L, Zhao S N, Ng M, Chan M Y, Yam V W W & Wong K M C, *J Am Chem Soc*, 141 (2019) 12863.
9 Chu W K, Yiu S M & Ko C C, *Organometallics*, 33 (2014) 6771.
10 Kwon Y, Han S H, Yu S, Lee J Y & Lee K M, *J Mater Chem C*, 6 (2018) 4565.
11 Li G J, Zhao X D, Fleetham T, Chen Q D, Zhan F, Zheng J B, Yang Y F, Lou W W, Yang Y N, Fang K, Shao Z Z, Zhang Q S & She Y B, *Chem Mater*, 32 (2020) 537.
12 Adamovich V, Boudreault P L T, Esteruelas M A, Gomez-Bautista D, Lopez A M, Onate E & Tsai J Y, *Organometallics*, 38 (2019) 2738.
13 Liao J L, Devereux L R, Fox M A, Yang C C, Chiang Y C, Chang C H, Lee G H, & Chi Y, *Chem Eur J*, 24 (2018) 624.
14 Wang S M, Yang Q Q, Zhang B H, Zhao L, Xia D B, Ding J Q, Xie Z Y & Wang L X, *Adv Opt Mater*, 5 (2017) 1700514.
15 Okamura N, Nakamura T, Yagi S, Maeda T, Nakazumi H, Fujiwara H & Koseki S, *RSC Adv*, 6 (2016) 51435.
16 Choi W H, Tan G P, Sit W Y, Ho C L, Chan C Y H, Xu W W, Wong W Y & So S K, *Org Electron*, 24 (2015) 7.
17 Li H, Yin Y M, Cao H T, Sun H Z, Wang, L, Shan G G, Zhu D X, Su Z M & Xie W F, *J Organomet Chem*, 753 (2014) 55.
18 Wong W Y & Ho C L, *Coord Chem Rev*, 253 (2009) 1709.
19 Lamansky S, Djurovich P, Murphy D, Abdel-Razzaq F, Lee H E, Adachi C, Burrows P E, Forrest S R & Thompson M E, *J Am Chem Soc*, 123 (2001) 4304.
20 Traskovskis K, Ruduss A, Kokars V, Mihailovs I, Lesina N & Vembris A, *New J Chem*, 43 (2019) 37.
21 Chen Z, Wang L Q, Ho C L, Chen S M, Suramitr S, Plucksacholatarn A, Zhu N Y, Hannongbua S & Wong WY, *Adv Opt Mater*, 6 (2018) 1800824.
22 Zhou X W, Burn P L & Powell B J, *J Chem Phys*, 146 (2017) 174305.
23 Shang X H, Han D M, Zhou D F & Zhang G, *New J Chem*, 41 (2017) 1645.
24 Bejoymohandas K S, Kumar A, Varughese S, Varathan E, Subramaniand V & Reddy M L P, *J Mater Chem C*, 3 (2015) 7405.
25 Liao J L, Chi Y, Sie Z T, Ku C H, Chang C H, Fox M A, Low P J, Tseng M R & Lee G H, *Inorg Chem*, 54 (2015) 10811.
26 Hohenberg P & Kohn W, *Phys Rev*, 136 (1964) B864.
27 Adamo C & Barone V, *J. Chem. Phys*. 110 (1999) 6158.
28 Hay P J & Wadt W R, *J Chem Phys*, 82 (1985) 284.
29 Hay P J & Wadt W R, *J Chem Phys*, 82 (1985) 299.
30 Frisch M J, Trucks G W, Schlegel H B, Scuseria G E, Robb M A, Cheeseman J R, Scalmani G, Barone V, Mennucci B, Petersson G A, Nakatsuji H, Caricato M, Li X, Hratchian H P, Izmaylov A F, Bloino J, Zheng G, Sonnenberg J L, Hada M, Ehara M, Toyota K, Fukuda R, Hasegawa J, Ishida M, Nakajima T, Honda Y, Kitao O, Nakai H, Vreven T, Montgomery J A, Peralta J E, Ogliaro F, Bearpark M, Heyd J J, Brothers E, Kudin K N, Staroverov V N, Kobayashi R, Normand J, Raghavachari K, Rendell A, Burant J C, Iyengar S S, Tomasi J, Cossi M, Rega N, Millam N J, Klene M, Knox J E, Cross J B, Bakken V, Adamo C, Jaramillo J, Gomperts R, Stratmann R E, Yazyev O, Austin A J, Cammi R, Pomelli C, Ochterski J W, Martin R L, Morokuma K, Zakrzewski V G, Voth G A, Salvador P, Dannenberg J J, Dapprich S, Daniels A D, Farkas O, Foresman J B, Ortiz, J V, Cioslowski J & Fox D J, Gaussian 09, Gaussian Inc, Wallingford CT, 2009.
31 O'Boyle N M, Tenderholt A L & Langner K M, *J Comput Chem*, 29 (2008) 839.
32 Świderek K & Paneth P, *J Phys Org Chem*, 22 (2009) 845.